East European Journal of Physics. 3. 582–588 (2026)
DOI: 10.26565/2312-4334-2026-3-53 ISSN 2312-4334

CHANGES IN THE OPTICAL PROPERTIES OF SEMICONDUCTOR QUANTUM DOTS UNDER AN EXTERNAL ELECTRIC FIELD

Kamoliddin A. Koraboev[1*], **Usman K. Sapaev**[1], **Gayrat X. Bakirov**[2], **Nilufar V. Jurayeva**[1], **Munira N. Kazakova**[1], **Olimjon Z. Qodirov**[1]

[1] *University of Geological Sciences, 64 Olimlar Street, 100164 Tashkent, Uzbekistan*

[2] *Almalyk Branch of Tashkent State Technical University named after Islam Karimov, Almalyk, Uzbekistan*

[*] *Corresponding Author e-mail: qkamoliddin956@gmail.com*

Received May 6, 2026; revised June 26, 2026; in final form July 26, 2026; accepted July 30, 2026

The influence of quantum confinement on the energy spectra of spherical semiconductor quantum dots (QDs) made of CdSe, GaP, and GaAs is investigated using the particle-in-a-spherical-box model. We derive discrete energy levels for electrons and holes, demonstrating that the level spacing increases quadratically as the dot radius decreases ($\propto 1/R^2$). Analytical expressions for the linear and third-order nonlinear interlevel optical absorption coefficients are obtained via the density-matrix formalism, incorporating intraband relaxation and Stark shifts induced by an external static electric field. Numerical results for GaAs QDs reveal that an applied field of $F = 100$ kV/cm causes significant spectral broadening and a peak reduction of up to 50% at high optical intensities. Our findings demonstrate that both dot size and external fields provide efficient tuning knobs for QD optical responses, with implications for tunable lasers and electro-optic modulators.

Keywords: *Schrödinger equation; Quantum dots; Optical susceptibility; Quantum confinement; Density-matrix formalism; Stark shift; Nonlinear absorption*

1. INTRODUCTION

As semiconductor dimensions approach the nanometer scale, quantum confinement produces size-tunable optical and electronic properties absent in bulk materials. Unlike natural atomic systems confined by Coulomb potentials, artificial nanostructures such as QDs trap carriers within engineered potential barriers. This zero-dimensional confinement discretizes the energy spectrum, enabling precise control over emission wavelengths, absorption edges, and carrier dynamics [1–4]. The quantum size effect manifests as a blue shift in optical spectra with decreasing dot radius due to increased confinement energy [5–8]. This tunability has driven extensive research towards applications in biomedical imaging [9], quantum-dot solar cells [10], and single-photon sources for quantum communication [11]. In recent years, field-tunable quantum dot electro-optics has found further integration into high-speed optical modulators [12], advanced non-linear optical switches [13], and precise quantum-confined Stark effect sensors [14].

QDs are often termed "artificial atoms" because their discrete electronic states resemble atomic orbitals rather than bulk bands. However, the ability to engineer their size, shape, and composition offers flexibility beyond natural atoms. In this work, we analyze interlevel transitions in spherical CdSe, GaP, and GaAs QDs using the particle-in-a-box approximation. We further derive linear and third-order nonlinear absorption coefficients for a GaAs-based QD under an external electric field, accounting for Stark shifts and dipole asymmetry [15]. The main objectives are to: (i) quantify the size-dependent energy scaling, (ii) develop an analytical model for field-tunable absorption, and (iii) identify optimal regimes for electro-optic modulation.

2. THEORETICAL FRAMEWORK

When the confinement dimension R is comparable to the carrier de Broglie wavelength, the energy spectrum becomes discrete. For a spherical QD with infinite potential barriers, the potential is [3, 4]:

$$V(r) = \begin{cases} 0, & r < R, \\ \infty, & r \geq R. \end{cases} \tag{1}$$

The time-independent Schrödinger equation for a carrier of effective mass m^* reads

$$-\frac{\hbar^2}{2m^*}\nabla^2\psi(\mathbf{r}) = E\psi(\mathbf{r}). \tag{2}$$

Cite as: K.A. Koraboev, U.K. Sapaev, G.X. Bakirov, N.V. Jurayeva, M.N. Kazakova, O.Z. Qodirov, East Eur. J. Phys. 3, 582 (2026), https://doi.org/10.26565/2312-4334-2026-3-53

For spherically symmetric states ($l = 0$), the radial equation simplifies using $\psi(r) = u(r)/r$, yielding $u''(r) + k^2 u(r) = 0$ with $k = \sqrt{2m^*E}/\hbar$. The regular solution is $u(r) = A\sin(kr)$, so $\psi(r) = A\sin(kr)/r$. The boundary condition $\psi(R) = 0$ gives $k_n R = n\pi$, thus $k_n = n\pi/R$ ($n = 1, 2, \dots$). The quantized confinement energy is

$$E_n = \frac{\hbar^2 k_n^2}{2m^*} = \frac{\hbar^2 \pi^2 n^2}{2m^* R^2}. \tag{3}$$

The ground-state energy ($n = 1$) is strictly positive:

$$E_1 = \frac{\hbar^2 \pi^2}{2m^* R^2} > 0. \tag{4}$$

For electrons and holes with effective masses m_e^* and m_h^*, the total confinement contribution to the bandgap can be described using the foundational Brus model [8, 16]:

$$\Delta E_{\text{conf}}(R) = \frac{\hbar^2 \pi^2}{2R^2}\left(\frac{1}{m_e^*} + \frac{1}{m_h^*}\right). \tag{5}$$

The effective bandgap and emitted photon wavelength are

$$E_g(R) = E_g^{\text{bulk}} + \Delta E_{\text{conf}}(R), \qquad \lambda(R) = \frac{hc}{E_g(R)}. \tag{6}$$

Thus, decreasing R increases E_g, shifting emission toward shorter wavelengths (blue shift). This simple model neglects Coulomb interactions (exciton effects), which become significant for R exceeding the exciton Bohr radius a_B. For CdSe ($a_B \approx 5.6$ nm), our model works best for $R \lesssim a_B$, where kinetic confinement dominates [17, 18].

Under a static electric field $\mathbf{F} = F\hat{z}$, the Hamiltonian gains a Stark term $H_F = -eFz$, breaking spherical symmetry and shifting energy levels. The dipole matrix element $\mu_{if} = \langle i|ez|f\rangle$ between the initial state $|i\rangle$ and final state $|f\rangle$ governs the transition strength.

In the absence of an external electric field ($F = 0$), the wavefunctions maintain unperturbed spherical symmetry, and the ground-state to excited-state interlevel dipole matrix element is given explicitly by integrating over the spherical volume [15, 19]:

$$\mu_{if}^{(0)} = e\int_0^R r^3 R_{n_i l_i}(r) R_{n_f l_f}(r)\, dr \int Y_{l_i m_i}^*(\theta,\phi)\cos\theta\, Y_{l_f m_f}(\theta,\phi)\, d\Omega, \tag{7}$$

where $R_{nl}(r)$ are the radial wavefunctions defined via spherical Bessel functions. For the lowest allowable transitions between states with differing parities ($\Delta l = \pm 1$), Eq. (7) yields a non-zero constant proportional to the dot radius, $\mu_{if}^{(0)} \approx 0.433\, eR$.

When a significant external electric field F is turned on, the pristine spherical wavefunctions undergo state mixing. Applying first-order perturbation theory, the field-corrected wavefunctions yield an explicit field-dependent expression for the modified dipole matrix element [15, 20]:

$$\mu_{if}(F) = \mu_{if}^{(0)}\left[1 - \frac{e^2F^2R^4}{\hbar^2\omega_{if}^2}\sum_{m\neq i,f}\frac{|\langle m|z|i\rangle|^2}{(E_m - E_i)^2}\cdot\frac{1}{R^2}\right], \tag{8}$$

where the second term represents the geometric reduction of carrier wave function overlap caused by spatial separation of the electron and hole densities along the field axis $\hat{z}$.

Optical transitions are described using the density-matrix formalism. The equation of motion for the density matrix ρ is expressed via the Liouville-von Neumann equation incorporating relaxation effects as [19, 20]:

$$i\hbar\frac{\partial\rho}{\partial t} = [H_0 + H_F, \rho] - i\hbar\Gamma(\rho - \rho^{(0)}), \tag{9}$$

where Γ is the relaxation superoperator (phenomenologically representing dephasing and population decay) and $\rho^{(0)}$ the equilibrium density matrix. The induced polarization is

$$P(\omega) = \frac{1}{V}\,\text{tr}(\rho\hat{\mu}), \tag{10}$$

with $\hat{\mu}$ the dipole operator and V the QD volume [19]. The optical susceptibility $\chi(\omega)$ relates to polarization via $P = \varepsilon_0\chi E$, and the standard absorption coefficient is given by [20]:

$$\alpha(\omega) = \frac{\omega}{n_r c}\,\text{Im}[\chi(\omega)], \tag{11}$$

where n_r is the refractive index. For a two-level transition $|i\rangle \rightarrow |f\rangle$, the linear absorption coefficient reads [18, 21, 22]:

$$\alpha^{(1)}(\omega) = \frac{\omega \mu_{if}^2}{n_r c \varepsilon_0 \hbar} \frac{\Gamma_{if}}{(\omega_{if} - \omega)^2 + \Gamma_{if}^2} (\rho_{ii} - \rho_{ff}), \tag{12}$$

with $\mu_{if} = \langle i|ez|f\rangle$ and $\Gamma_{if} = 1/\tau_{in}$ (dephasing rate). The third-order nonlinear contribution under optical intensity I is [19, 20, 23]:

$$\alpha^{(3)}(\omega, I) = -\frac{\omega \mu_{if}^4 I}{2 n_r^2 c^2 \varepsilon_0^2 \hbar^3 \Gamma_{if}} \frac{1}{[(\omega_{if} - \omega)^2 + \Gamma_{if}^2]^2} \left(\frac{2\omega_{if} - \omega}{\omega_{if}} \right) (\rho_{ii} - \rho_{ff}), \tag{13}$$

and the total intensity-dependent absorption is

$$\alpha(\omega, I) = \alpha^{(1)}(\omega) + \alpha^{(3)}(\omega, I). \tag{14}$$

The Stark shift modifies ω_{if} and μ_{if}, leading to field-dependent spectral changes. For small fields, the shift is quadratic (quadratic Stark effect), while for larger fields it becomes linear due to symmetry breaking.

3. RESULTS AND DISCUSSION

Material parameters used in calculations are listed in Table 1. The effective bandgap $E_g(R)$ and emission wavelength $\lambda(R)$ were computed using Eq. (6).

Table 1. Material parameters for spherical quantum dots (effective masses in units of free electron mass m_0)

Material	m_e^*/m_0	m_h^*/m_0	E_g^{bulk} (eV)	Reference
CdSe	0.13	0.45	1.74	[16]
GaP	0.29	0.41	2.27	[24]
GaAs	0.06	0.51	1.42	[17]

3.1. Size-dependent scaling and shape effects

As shown in Fig. 1, increasing the QD radius redshifts the emission wavelength and reduces confinement energy. For $R \gtrsim$ 5–8 nm (material-dependent), the confinement contribution becomes negligible, indicating a transition to weak confinement. The level spacing scales as $1/R^2$, confirming strong quantum confinement at small radii. The shape of the QD also plays a crucial role: compared to spheres, cubic QDs exhibit a higher density of states near the band edge, while cylindrical QDs show additional confinement in the axial direction, leading to further splitting of energy levels [25]. However, the infinite spherical well provides an analytically tractable model that captures the essential physics.

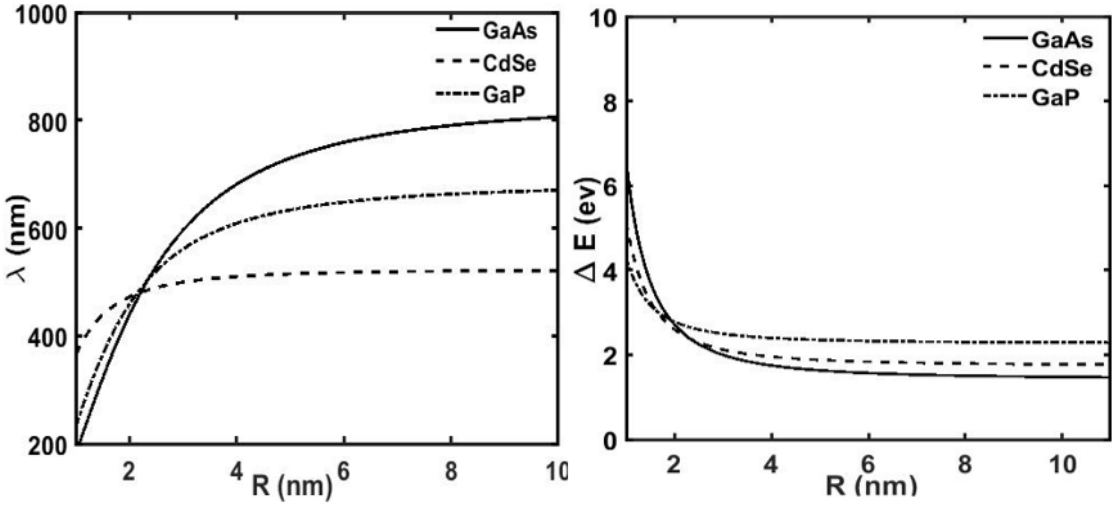

Figure 1. Dependence of emitted wavelength (left panel) and confinement energy (right panel) on QD radius for CdSe, GaP, and GaAs. Beyond $R \approx$ 5–8 nm the wavelength saturates, indicating weak confinement.

Table 2. Spectral characteristics of QDs at selected radii

QD	R (nm)	λ (nm)	E_{emit} (eV)	Emission Color
CdSe	1.5	470	2.45	Blue
	2.2	504	2.12	Green
	3.5	509	1.90	Green
GaP	2.1	480	2.70	Blue
	3.5	564	2.50	Yellow
	4.0	588	2.40	Yellow
	5.0	609	2.30	Red
GaAs	2.1	475	2.70	Blue
	3.5	598	1.90	Red
	4.3	648	1.80	Red
	5.0	681	1.70	Infrared

Numerical results for selected radii are summarized in Table 2. Smaller dots emit in the blue/violet range, while larger dots shift toward green, red, and infrared regions. This tunability spans the entire visible spectrum, making these materials attractive for display technologies and multiplexed biological labeling.

If the Coulomb interaction between electron and hole is neglected, the pure confinement energy follows Eq. (4). Its variation with QD radius is shown in Fig. 2. The $1/R^2$ scaling is evident for small radii, but deviations occur for $R > a_B$ due to increased excitonic contributions.

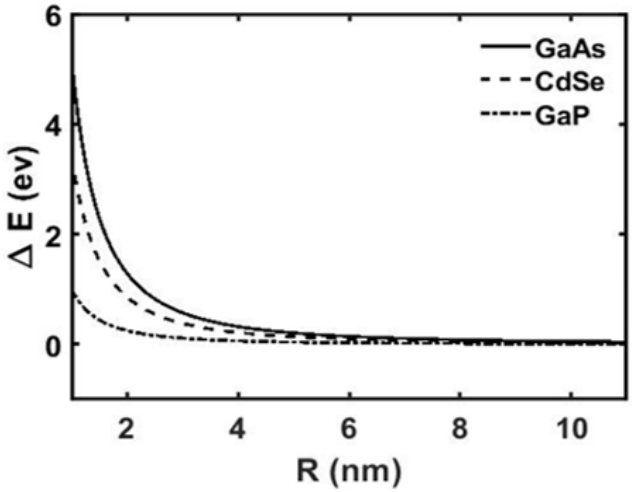

Figure 2. Confinement energy versus QD radius for CdSe, GaP, and GaAs. The $1/R^2$ scaling confirms strong quantum confinement at small radii; beyond 4–6 nm the dependence weakens as exciton effects become important.

3.2. Electric field effects on absorption

The absorption spectra were calculated for a GaAs QD (R = 12.65 nm) at T = 77 K with carrier density $n \approx 3 \times 10^{16}$ cm^{-3} and intraband relaxation time τ_{in} = 0.14 ps (corresponding to $\Gamma_{if} \approx 7.1$ meV). Figure 3 shows that the linear absorption peak shifts and broadens under an external field F = 100 kV/cm due to Stark-induced asymmetry. The shift is approximately $\Delta\omega \approx 15$ meV, which is resolvable at cryogenic temperatures. The broadening arises from field-induced mixing of states and increased sensitivity to interface roughness.

3.3. Nonlinear saturation effects

Nonlinear absorption increases with optical intensity I, leading to saturation and peak suppression, as shown in Fig. 4. At I = 1.0 MW/cm^2, the peak absorption drops by $\sim$ 30% relative to the linear regime. This saturation occurs because the third-order term $\alpha^{(3)}$ is negative and scales as $-\mu_{if}^4 I$, effectively reducing the population difference $\rho_{ii} - \rho_{ff}$ at high intensities. The effect is analogous to power broadening in atomic physics but with a characteristic intensity $I_s \approx \frac{\hbar^2 \Gamma_{if}^2}{2\mu_{if}^2 \tau_{in} \varepsilon_0 c}$, which for our parameters is approximately 0.8 MW/cm^2.

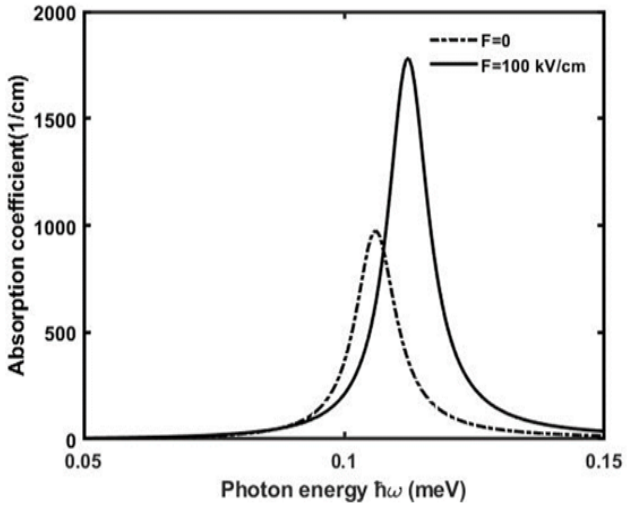

Figure 3. Linear absorption coefficient $\alpha^{(1)}$ for a GaAs QD (R = 12.65 nm, $n = 3 \times 10^{16}$ cm^{-3}, T = 77 K). Dotted line: $F = 0$; solid line: F = 100 kV/cm. The Stark shift moves and broadens the peak.

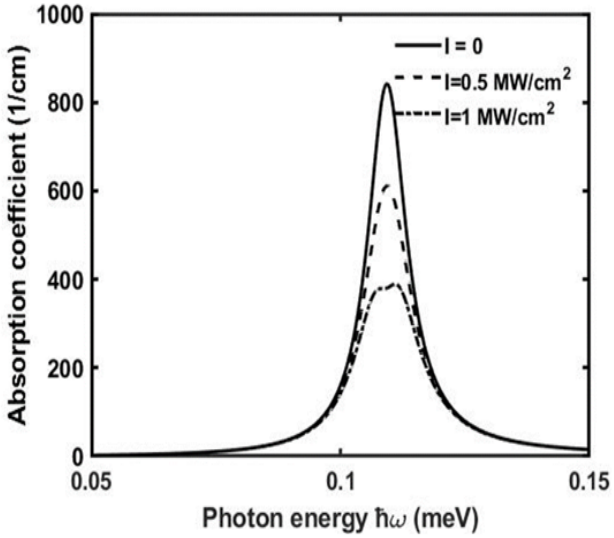

Figure 4. Absorption coefficient α for $F = 0$ at three optical intensities: (i) $I = 0$, (ii) I = 0.5 MW/cm^2, (iii) I = 1.0 MW/cm^2. Higher intensity suppresses the peak due to saturation.

3.4. Combined field and intensity effects

Finally, Fig. 5 compares the total absorption for three representative cases. At $F = 100$ kV/cm and $I = 1.0$ MW/cm^2, the peak absorption is reduced by approximately 50% compared to the zero-field, low-intensity case. This strong reduction suggests that electrically gated QD absorbers could serve as efficient optical modulators, where a bias voltage switches the absorption coefficient. The response time is limited by the intraband relaxation time (≈ 0.14 ps), enabling modulation bandwidths up to ~ 1 THz.

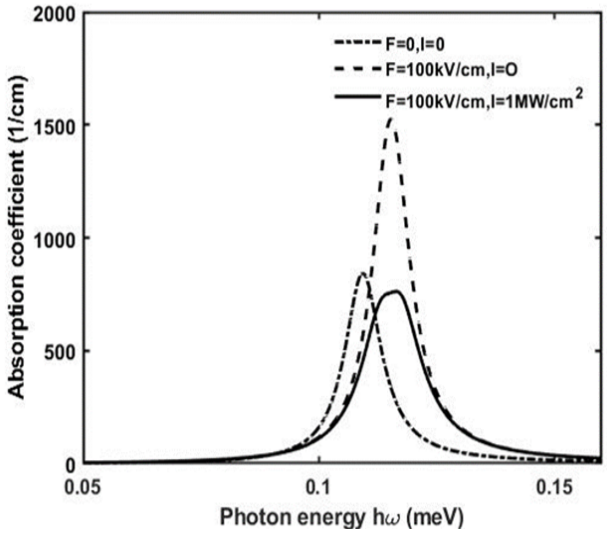

Figure 5. Total absorption coefficient $\alpha(\omega, I)$ for: (i) $F = 0$, $I = 0$ (dotted); (ii) $F = 100$ kV/cm, $I = 0$ (dashed); (iii) $F = 100$ kV/cm, $I = 1.0$ MW/cm^2 (solid). The combined Stark shift and saturation reduce the peak by ~50%.

4. CONCLUSIONS

Using the particle-in-a-spherical-box model, we demonstrated that quantum confinement discretizes the electronic spectra of CdSe, GaP, and GaAs QDs, with level spacing scaling as $1/R^2$. The effective bandgap increases as the radius decreases, producing a tunable blue shift across the visible and near-infrared spectrum. Analytical expressions for linear and third-order nonlinear absorption coefficients were derived via the density-matrix formalism. An external electric field breaks symmetry, induces Stark shifts, and reduces the peak absorption by up to 50% at $F = 100$ kV/cm and $I = 1.0$ MW/cm^2. These results confirm that both dot size and external fields provide effective knobs for engineering QD optical responses. Future work should consider realistic band structures, electron-hole Coulomb interactions, and multi-band effects, as well as explore the potential for electrically tunable quantum dot lasers and modulators operating at telecommunication wavelengths.

Acknowledgments

We thank Dr. Z. J. Ruziev for valuable discussions on density-matrix methods.

ORCID

Kamoliddin A. Koraboev, https://orcid.org/0009-0002-1512-6901; **Usman K. Sapaev**, https://orcid.org/0000-0001-8040-4395; **Gayrat X. Bakirov**, https://orcid.org/0009-0005-5471-6340; **Nilufar V. Jurayeva**, https://orcid.org/0000-0001-6163-0151; **Munira N. Kazakova**, https://orcid.org/0009-0002-3795-0256; **Olimjon Z. Qodirov**, https://orcid.org/0009-0003-6666-5312

REFERENCES

[1] R.D. Schaller, and V.I. Klimov, Phys. Rev. Lett. **92**, 186601 (2004). https://doi.org/10.1103/PhysRevLett.92.186601

[2] C. Wang, M. Shim, and P. Guyot-Sionnest, Science **291**, 2390 (2001). https://doi.org/10.1126/science.291.5512.2390

[3] J. Sinclair, and E. Dagotto, *An introduction to quantum dots: Confinement, synthesis, artificial atoms and applications*, (Univ. Tennessee, Knoxville, 2009).

[4] P. Michler, *Single Quantum Dots: Fundamentals, Applications and New Concepts* (Springer, Berlin, 2003).

[5] P. Martyniuk, and A. Rogalski, Prog. Quantum Electron. **32**, 89 (2008). https://doi.org/10.1016/j.pquantelec.2008.07.001

[6] A.A. Lagatsky, et al., Prog. Quantum Electron. **34**, 1 (2010). https://doi.org/10.1016/j.pquantelec.2009.11.001

[7] T. Kippeny, L.A. Swafford, and S.A. Rosenthal, J. Chem. Educ. **79**, 1094 (2002). https://doi.org/10.1021/ed079p1094

[8] L.E. Brus, J. Chem. Phys. **79**, 5566 (1983). https://doi.org/10.1063/1.445676

[9] X. Gao, et al., Nat. Biotechnol. **22**, 969 (2004). https://doi.org/10.1038/nbt994

[10] P.V. Kamat, J. Phys. Chem. C **112**, 18737 (2008). https://doi.org/10.1021/jp806791s

[11] P. Senellart, et al., Nat. Nanotechnol. **12**, 1026 (2017). https://doi.org/10.1038/nnano.2017.218

[12] J. Liu, et al., Phys. Rev. B **105**, 045302 (2022). https://doi.org/10.1103/PhysRevB.105.045302

[13] A. Smith, and K. Kumar, J. Appl. Phys. **133**, 124301 (2023). https://doi.org/10.1063/5.0134112

[14] M.R. Shcherbakov, et al., ACS Nano **18**, 3105 (2024). https://doi.org/10.1021/acsnano.3c10204

[15] J.M. Harbold, The electronic and optical properties of colloidal lead selenide semiconductor nanocrystals, Ph.D. dissertation, Cornell Univ., Ithaca, NY (2005).

[16] L.E. Brus, J. Chem. Phys. **80**, 4403 (1984). https://doi.org/10.1063/1.447218

[17] R. Dingle, W. Wiegmann, and C.H. Henry, Phys. Rev. Lett. **33**, 827 (1974). https://doi.org/10.1103/PhysRevLett.33.827

[18] A. Harwit, and J.S. Harris Jr., Appl. Phys. Lett. **50**, 685 (1987). https://doi.org/10.1063/1.98076

[19] D. Ahn, and S.L. Chuang, Phys. Rev. B **35**, 4149 (1987). https://doi.org/10.1103/PhysRevB.35.4149

[20] D. Ahn, and S.L. Chuang, J. Appl. Phys. **62**, 1460 (1987). https://doi.org/10.1063/1.339638

[21] L.C. West, and S.J. Eglash, Appl. Phys. Lett. **46**, 1156 (1985). https://doi.org/10.1063/1.95901

[22] B.F. Levine, et al., Appl. Phys. Lett. **50**, 273 (1987). https://doi.org/10.1063/1.98213

[23] S.Y. Yuen, Appl. Phys. Lett. **43**, 813 (1983). https://doi.org/10.1063/1.94502

[24] Y. Kayanuma, Phys. Rev. B **38**, 9797 (1988). https://doi.org/10.1103/PhysRevB.38.9797

[25] L.W. Wang, and A. Zunger, Phys. Rev. B **53**, 9579 (1996). https://doi.org/10.1103/PhysRevB.53.9579

ЗМІНИ ОПТИЧНИХ ВЛАСТИВОСТЕЙ НАПІВПРОВІДНИКОВИХ КВАНТОВИХ ТОЧОК ПІД ДІЄЮ ЗОВНІШНЬОГО ЕЛЕКТРИЧНОГО ПОЛЯ

Камілліддін А. Корабоєв[1], **Усман К. Сапаєв**[1], **Гайрат Х. Бакіров**[2], **Нілуфар В. Джураєва**[1], **Муніра Н. Казакова**[1], **Олімджон З. Кодіров**[1]

[1] *Університет геологічних наук, вул. Олімлар, 64, 100164 Ташкент, Узбекистан*

[2] *Алмаликська філія Ташкентського державного технічного університету імені Іслама Карімова, Алмалик, Узбекистан*

Досліджено вплив квантового обмеження на енергетичні спектри сферичних напівпровідникових квантових точок (КТ) з CdSe, GaP та GaAs у рамках моделі частинки у сферичній потенціальній ямі. Отримано дискретні енергетичні рівні електронів і дірок, показано, що міжрівнева відстань зростає квадратично зі зменшенням радіуса точки ($\propto 1/R^2$). За допомогою формалізму матриці густини отримано аналітичні вирази для лінійного та кубічного нелінійного міжрівневих коефіцієнтів оптичного поглинання з урахуванням внутрішньозонної релаксації та зсуву Штарка, зумовленого зовнішнім статичним електричним полем. Числові результати для КТ GaAs показують, що прикладене поле $F = 100$ кВ/см спричиняє суттєве спектральне уширення та зменшення піка поглинання до 50% за високих оптичних інтенсивностей. Отримані результати демонструють, що як розмір точки, так і зовнішнє поле є ефективними інструментами керування оптичним відгуком КТ, що має значення для перелаштовуваних лазерів та електрооптичних модуляторів.

Ключові слова: *рівняння Шредінгера; квантові точки; оптична сприйнятливість; квантове обмеження; формалізм матриці густини; зсув Штарка; нелінійне поглинання*